All-Polystyrene 3D-Printed Electrochemical Device with Embedded Carbon Nanofiber – Graphite – Polystyrene Composite Conductor

Zuhayr Rymansaib,[1] Pejman Iravani,*[1] Edward Emslie,[2]
Martina Medvidović-Kosanović,[3] Milan Sak-Bosnar,[3] Raquel Verdejo [4], Frank Marken*[2]

[1] *Department of Mechanical Engineering, University of Bath, Bath BA2 7AY, UK*

[2] *Department of Chemistry, University of Bath, Bath BA2 7AY, UK*

[3] *Department of Chemistry, University of Osijek, Cara Hadrijana 8A, HR- 31000, Osijek, Croatia*

[4] *Institute of Polymer Science and Technology, ICTP-CSIC, C/ Juan de la Cierva, 3, 28006, Madrid, Spain*

Abstract

Carbon nanofibres (CNFs) and graphite flake microparticles were added to thermoplastic polystyrene polymer with the aim of making new conductive blends suitable for 3D-printing. Various polymer/carbon blends were evaluated for suitability as printable, electroactive material. An electrically conducting polystyrene composite was developed and used with commercially available polystyrene (HIPS) to manufacture electrodes suitable for electrochemical experiments. Electrodes were produced and evaluated for cyclic voltammetry of aqueous 1,1'-ferrocenedimethanol and differential pulse voltammetry detection of aqueous Pb^{2+} via anodic stripping. A polystyrene/ CNF/ graphite (80/10/10 wt%) composite provides good conductivity and a stable electrochemical interface with well-defined active geometric surface area. The printed electrodes form a stable interface to the polystyrene shell, gives good signal to background voltammetric responses, and are reusable after polishing.

Keywords: manufacturing, device prototyping, trace analysis, polymer formulation, sensor architecture.

Graphical Abstract:

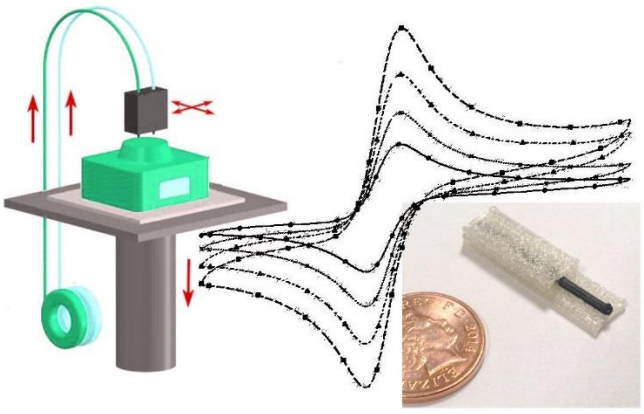

1. Introduction

Rapid prototyping and manufacturing techniques have been revolutionised by new 3D-printing technologies based, for example, on ink jet [1], fused filament [2], or laser additive deposition [3] methods. Complex structures are produced reproducibly and optimised within short periods of development time. “Bioprinting” offers access to complex tissue and biological structures [4]. For synthetic chemistry [5] as well as for electrochemistry there is a need for rapid prototyping, in particular for widely used sensors based on carbon composites. Approaches proposed so far include for example mixing of silicone sealant with carbon black as printable electroactive material [6]. However, unknown additives in commercially available silicones can cause interference in particular in analytical applications. New composite formulations are desirable to give good printing performance and good electrical and electrochemical characteristics. Recently significant progress has been made in printing milli-fluidic devices [7], metal-alloy based conductor structures [8,9], “carbomorph” based conductive composites for electronic sensors [10], metal structures produced by electroless deposition onto 3D-printed objects [11], graphene-based composite components [12], and for the printing of solid phase micro extraction devices [13]. In some cases 3D-printed devices were employed with conventional electrodes [14,15], although the real benefit in the 3D-printing method is in the printing of complete systems including electrodes and device.

Carbon is ubiquitous in electrochemistry and in electroanalysis [16], available in various forms such as cloth, rods, fibres and the like. Nanocarbons such as carbon nanotubes [17], nanofibers [18], nanoparticles [19], or graphenes [20] have been developed into composite electrode materials. Inert, yet electrically conductive, carbon nano-composites can provide a cheap alternative to noble metals. Compacted carbon nanofibers in polystyrene for applications in electroanalysis have been reported previously [21].

3D-printing gives access to low cost, rapid customisation and production of disposable devices [22]. A schematic of a typical printing device is shown in Figure 1A. A thermoplastic, such as polystyrene is supplied as filament into a heated nozzle and applied to the sample on a computer controlled x,y,z stage. Here we use additives including graphite flakes and carbon nanofibers to develop and manufacture a fully 3D-printed electrode based on polystyrene composites for voltammetric sensing in aqueous media and for heavy metal detection. A combination of carbon materials is employed in various polymers in order to achieve (i) sufficient electrical bulk conductivity, (ii) a reproducible and mechanically stable (polishable/reusable) and electrochemically reactive interface to aqueous solutions, and (iii) a good signal to background voltammetric response with insignificant capacitance due to ingress of solution phase into the carbon composite.

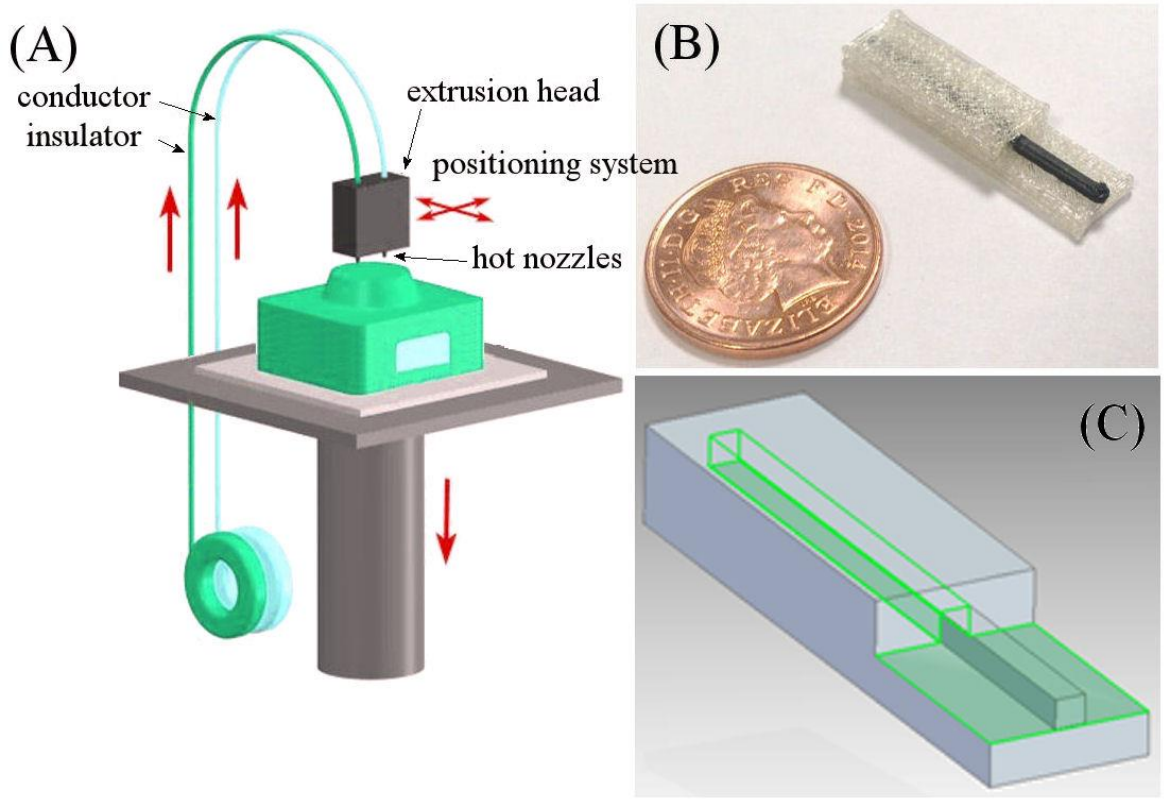

Figure 1. (A) Schematic diagram of a 3D printing set up with two feeds (polystyrene insulator and polystyrene composite conductor) being printed through a hot nozzle system with positional controller. (B) Photograph of a printed polystyrene – nanocarbon composite electrode. (C) Multi-part electrode being designed in CAD software.

2. Experimental

2.1. Materials & Chemical Reagents

Reagents employed in this study were toluene, acetone, acrylonitrile butadiene styrene (ABS) granules (Sabic MG94 resin, OS3DP.com), polylactic acid (PLA, Aldrich), polystyrene (HIPS) pellets (441147 Sigma-Aldrich), polycaprolactone (PCL) filament (Makerbot MP05188), graphene-PLA filament (Graphene 3D Lab, 3dfilaprint.com), polypropylene (PP) filament (NuNus 3D printer filaments), graphite flakes (28286-3 Sigma-Aldrich), Pyrograf III carbon nanofibres (PR-24-XT-HHT), paraffin wax (411671 Sigma-Aldrich), HNO_3, $Pb(NO_3)_2$, KNO_3, 1,1'-ferrocenedimethanol (all Aldrich).

2.2. Instrumentation

Electrochemical measurements were performed with a PGSTAT12 potentiostat (Autolab, NL). The counter and reference electrodes were a platinum wire and a KCl-saturated calomel (SCE) electrode (Radiometer, Ref401). Admittance measurements were performed on composite filaments with a Solartron 1296 (UK). Scanning electron microscopy (SEM) images were obtained with a JEOL SEM6480LV. All experiments were performed at a temperature of 20 ± 2 ^{o}C.

2.3. Procedures

Composite Thermoplastic Filament Fabrication. An amount of 5 g total (polymer and additives in the correct ratios) is weighed out. The polymer is first dissolved in 50 mL of an appropriate solvent (e.g. acetone for ABS and chloroform for PS) and stirred with a magnetic stirrer until fully dissolved. The additives are mixed in a separate container with 50 mL of the same solvent, and sonicated for 20

minutes. Containers were sealed to prevent solvent evaporation. The two mixtures are then combined in a single open container and placed on a heated magnetic stirrer at 50 °C in a fume cupboard until all the solvent has evaporated. After the complete evaporation of the solvent, the solid thermoplastic composite is placed in a heated (220 °C) aluminium barrel with a 2 mm orifice and extruded into lengths of composite conductive filament to be used for 3D-printing.

CAD Design and 3D-Printing. The electrode was designed as a multi-material part using a CAD package (Solid Edge ST6) (see Figure 1C). Electrode tip dimensions are 4.5 mm × 7.5 mm with a 0.81 mm × 0.81 mm active area in the centre. The CAD file is subsequently processed with open source software Slic3r to convert to printing commands. A 350 μm layer height was used resulting in 9 layers for printing of the complete electrode. The electrodes were then printed using a custom-built fused filament deposition 3D-printer equipped with two 0.5 mm extruders.

3. Results and Discussion

3.1. 3D-Filament Material Formulations and Optimisation

Crucial in the performance of the carbon composite material is the electrical conductivity. Admittance measurement results are shown in Figure 2D. Polystyrene with 10 wt% CNF and 10 wt% graphite exhibited the best electrical conductivity of the tested formulations (see Figure 2Di). Initially, a variety of polymer composites were produced and evaluated. It was found that when using low amounts (1-5 wt%) of carbon nanofibers (CNFs) the material would behave as dielectric rather than conductor (not shown) with the frequency dependency of the impedance/admittance characteristic of such highly resistive materials. Once the percolation threshold is exceeded, the carbon additives form a connective network and the material goes from being dielectric to conductive. The admittance is then independent of frequency up to typically 10^5 Hz (Figure 2D).

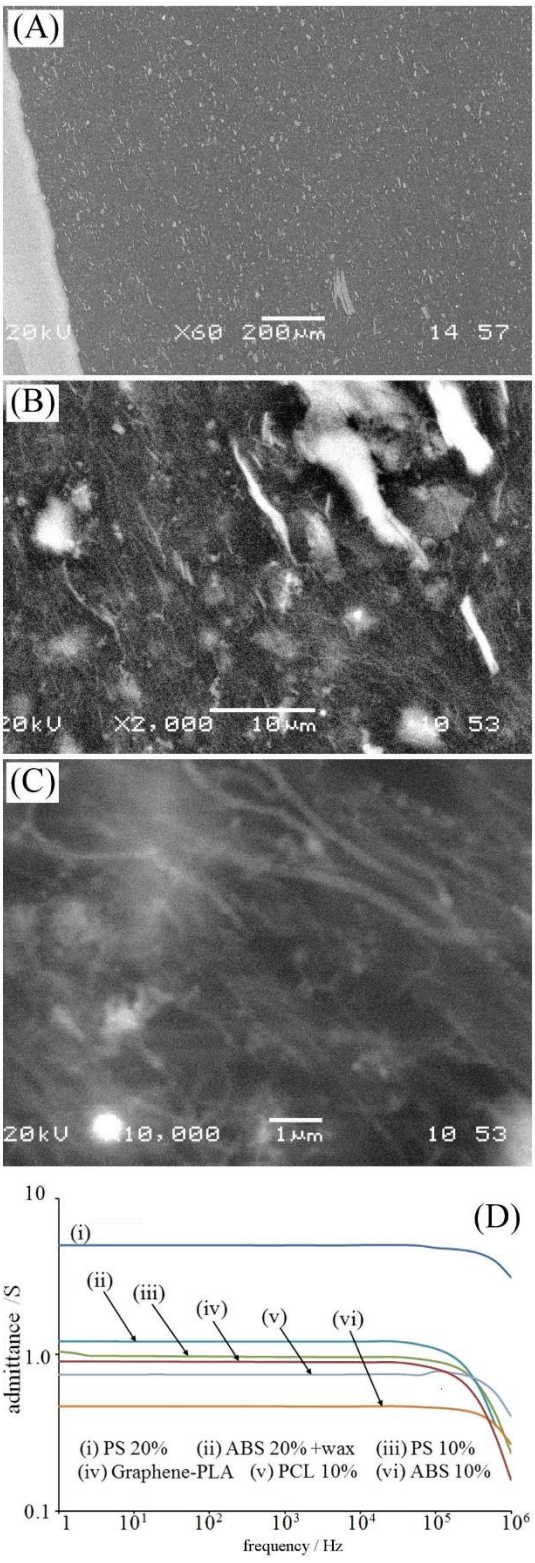

Figure 2. (A) Scanning electron micrographs (SEMs) for a composite filament produced from 80 wt% polystyrene, 10 wt% CNFs, 10 wt% graphite flakes. (B,C) Higher magnification images show the presence of typically 50-500 nm diameter CNFs and some graphite flakes of 2-12 μm diameter. (D) Admittance versus frequency plots for different composites showing relatively low resistance for 80 wt% polystyrene/ 10 wt% CNFs/ 10 wt% graphite flakes (i).

A minimum of 10 wt% CNFs had to be used to ensure that the conductivity of the electrode is sufficient for voltammetry, slightly more than previously reported percolation thresholds achieved in similar composites [23]. Attempts at additional CNF loading led to loss of plasticity and difficulty in using the filaments for 3D-printing. Instead, graphite micro-flakes of 2-12 μm diameter were added to further increase the conductivity of the composites, allowing the total carbon content to increase to 20 wt%, whilst remaining printable. Initial blends focused on producing carbon composites based on ABS or PCL, two widely used 3D-printing filaments. However, as can be seen from admittance readings in Figure 2D PS/CNF composites gave superior performance at similar CNF loading ratios. This was further improved by adding 10 wt% graphite. Additionally, ABS or PCL/CNF composites gave poor voltammetric response probably due to interfacial wetting effects (*vide infra*).

Multiple core/shell combinations were produced to investigate the effects of the active and inactive material. As ABS is hygroscopic, 2 wt% paraffin wax was added to the mixture to prevent water/analyte absorption during application. The resulting composite filament exhibited good electrical properties. Switching to PS, a non-hygroscopic polymer, meant that the wax component could be omitted. The PS composites gave the best conductivity results throughout, and were found to give greater conductivity than the commercially available graphene-PLA filaments (Figure 2Div). However, PS composites were substantially less flexible mechanically. Figure 2A shows a typical SEM image for a 80/10/10 wt% composite of polystyrene/CNFs/graphite flakes. The carbon nanofiber (CNF) component is visible with higher magnification (Figure 2B,C) as 50-500 nm diameter fibrous material. Carbon flakes or 2-12 μm appear as white particles.

3.2. Oxidation of 1,1'-Ferrocenedimethanol at 3D-Printed Polystyrene/CNF/Graphite Electrodes

In order to evaluate the electrochemical performance of polymer nanocomposites, cyclic voltammetry experiments were carried out using the printed electrodes with mechanically polished surface and with different core/shell combinations. Figure 3A shows an SEM image for the polished surface with the transition from the conducting polystyrene/CNF/graphite composite to the electrically insulating polystyrene clearly visible. Silver paint was applied to the electrode ends to give good electrical contacts before connecting as the working electrode in a conventional 3-electrode setup controlled by a potentiostat. Initially, PLA was explored for use as shell material, one commonly used for filament based 3D-printing, but the more hydrophilic nature of this material caused ingress of liquid into cavities. Polypropylene (PP) was thus evaluated as a non-hygroscopic shell material, however, printing with PP gave significant warping and inter-layer adhesion issues. Therefore, keeping shell and core-conductor materials the same is beneficial. Use of raw PS as shell material could not be achieved, due to its brittle nature. High Impact Polystyrene (HIPS) was thus used instead. For voltammetric testing in aqueous media, we used the oxidation of 0.2 mM 1,1 ferrocenedimethanol in aqueous 0.1 M potassium nitrate (KNO_3) solution as a well-defined one-electron redox reaction (equation 1).

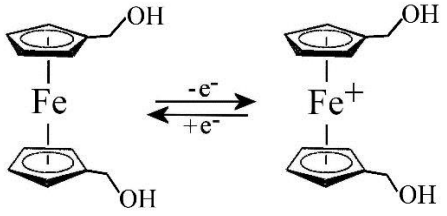

(1)

Data in Figure 3B show the typical reversible cyclic voltammetry characteristics for the oxidation of 1,1'-ferrocenedimethanol with a midpoint potential of $E_{mid} = ½ (E_{ox} + E_{red}) = 0.24$ V vs. SCE in good agreement with literature reports [24]. When comparing ABS/carbon and PS/carbon composites, both types of materials appear to be performing well. However, for ABS it was necessary to add a further 2 wt% paraffin wax component to suppress capacitive currents due to electrolyte ingress into the composite. Data in Figure 3C show that the voltammetric characteristics for polystyrene/ CNF/ graphite are even better (less capacitive background current) when avoiding the paraffin wax additive.

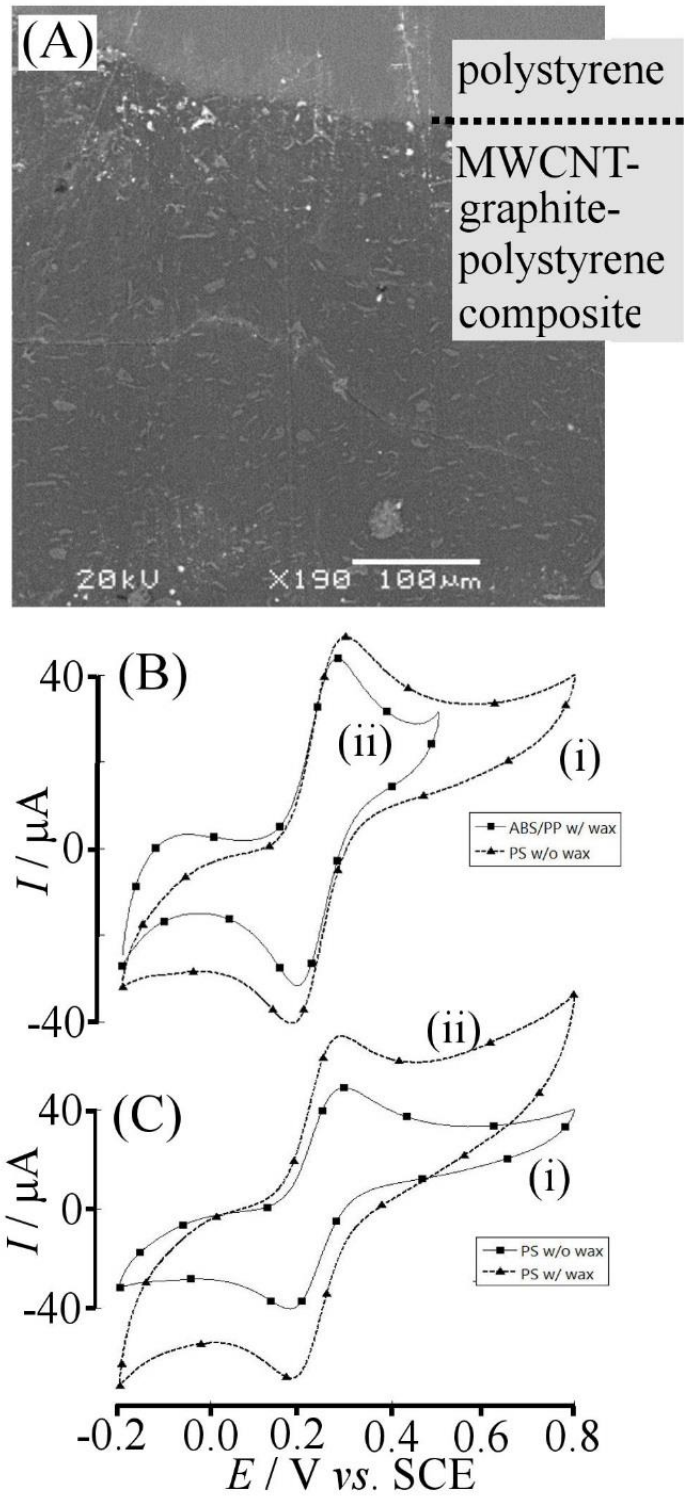

Figure 3. (A) Scanning electron micrograph (SEM) of a polystyrene – MWCNT-graphite-polystyrene composite electrode. (B) Cyclic voltammograms (scan rate 100 mVs^{-1}) for the oxidation of 0.2 mM 1,1'-ferrocenedimethanol in 0.1 M KNO_3 at (i) polystyrene/CNF/graphite and (ii) ABS/wax. (C) Cyclic voltammograms (scan rate 100 mV s^{-1}) for the oxidation of 0.2 mM 1,1'-ferrocenedimethanol in 0.1 M KNO_3 at (i) polystyrene/CNF/graphite and (ii) polystyrene/CNF/graphite/wax.

Next, the effect of the scan rate on the voltammetric oxidation peak response for the oxidation of 0.2 mM 1,1'-ferrocenedimethanol was investigated (see Figure 4). Figure 4B shows the well-defined linear characteristics of the plot for peak current versus square root of scan rate consistent with planar diffusion to a highly active electrode surface. The corresponding equation for the analysis of this diffusion limited peak current for the one-electron oxidation (equation 2) is known as Randles-Sevcik equation.

$$I_p = 0.446F^{3/2}Ac_{bulk}\sqrt{\frac{vD}{RT}} \qquad (2)$$

In this equation the peak current, I_p, is given by the Faraday constant, F, the geometric electrode area, A, the bulk concentration of 1,1'-ferrocnedimethanol, c_{bulk}, the scan rate, v, the diffusion coefficient, D, the gas constant, R, and the absolute temperature, T. With the slope of the plot in Figure 4B $slope = \frac{I_p}{\sqrt{v}} = 1.02 \times 10^{-6}$ A $V^{-1/2}$ $s^{1/2}$ and a literature value for the diffusion coefficient [25], $D = 0.64 \times 10^{-9}$ m^2 s^{-1}, only the geometry area of the 3D-printed electrode remains as free parameter and is therefore evaluated as $A = 7.3 \times 10^{-7}$ m^2 consistent with a square of 0.86 mm size in approximate agreement with the print size of the electrode.

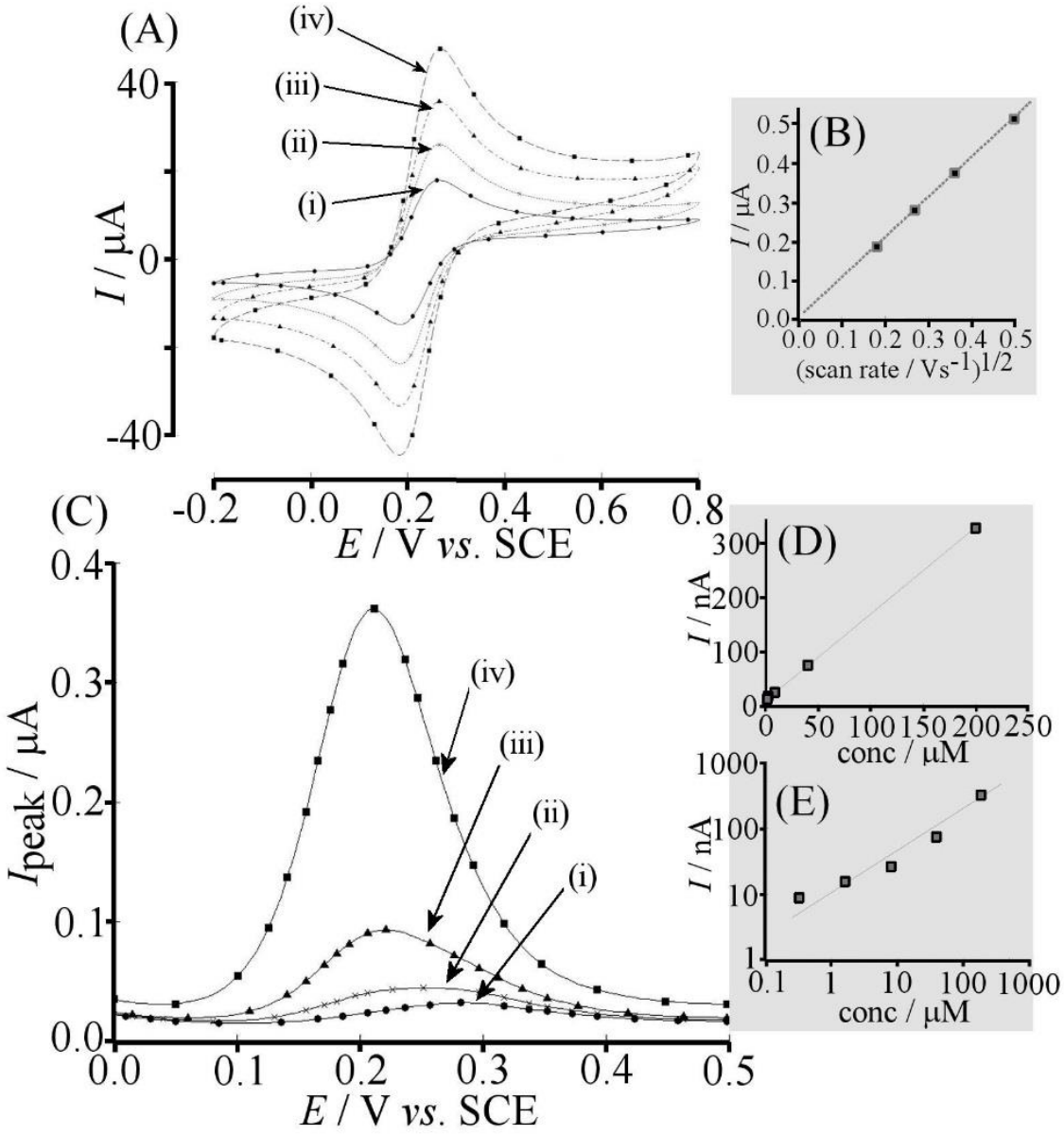

Figure 4. (A) Cyclic voltammograms (scan rate (i) 20, (ii) 50, (iii) 100, (iv) 200 mVs^{-1}) for the oxidation of 0.2 mM 1,1'-ferrocenedimethanol at a polystyrene/CNF/graphite electrode. (B) Plot of the peak current for oxidation versus the square root of scan rate. (C) Differential pulse voltammetry (DPV, modulation 25 mV, step potential 5 mV, modulation time 0.1 s) for the oxidation of (i) 1.6, (ii) 8, (iii) 40, (iv) 200 μM 1,1'-ferrocenedimethanol in 0.1 M KNO_3 at a polystyrene/CNF/graphite composite electrode. (D) Plot of the DPV peak current versus 1,1'-ferrocenedimethanol concentration and (E) double logarithmic plot.

The effect of lowering 1,1'-ferrocenedimethanol concentration on the voltammetric response was evaluated with differential pulse voltammetry (DPV). Data in Figure 4C shows peaks responses down to micromolar concentrations with apparently linear peak current versus concentration plot (Figure 4D). However, further inspection reveals (i) a shift in the peak position indicative of a change in

mechanism for example when adsorbed 1,1'-ferrocenedimethanol is detected and (ii) excess current in the low concentration range revealed by the double logarithmic plot in Figure 4E again indicative of adsorption effect. It is likely that for micromolar concentrations of 1,1'-ferrocenedimethanol some adsorption into the nanocomposite matrix occurs.

3.3. Reduction and Anodic Stripping Detection of Aqueous Pb^{2+} at 3D-Printed Polystyrene/CNF/Graphite Electrodes

An important application of 3D-printed carbon composite electrodes could be in trace metal detection in aqueous media [26,27,28], to test for contaminants, for example in natural in water systems [29] or in water wells [30]. Here we use $Pb(NO_3)_2$ (lead nitrate) in aqueous 0.1 M nitric acid as test analytical system. The reduction of Pb^{2+} leads to deposition and accumulation of Pb metal at the electrode surface and after sufficient accumulation a voltammetric stripping peak associated with the back-oxidation is observed (equation 3).

$$Pb^{2+}(aq) + 2\,e^- \rightleftharpoons Pb(s) \qquad (3)$$

Initially, a high concentration of Pb^{2+} is employed in order to explore the nucleation and deposition processes in aqueous 0.1 M nitric acid. With a deposition voltage of -1.0 V vs. SCE and deposition time 60 s, well-defined Pb stripping responses were observed. After measuring, the electrode is either re-used for multiple measurements or polished (on fine carborundum paper) to expose fresh electrode surface. Both methods produce reliable data.

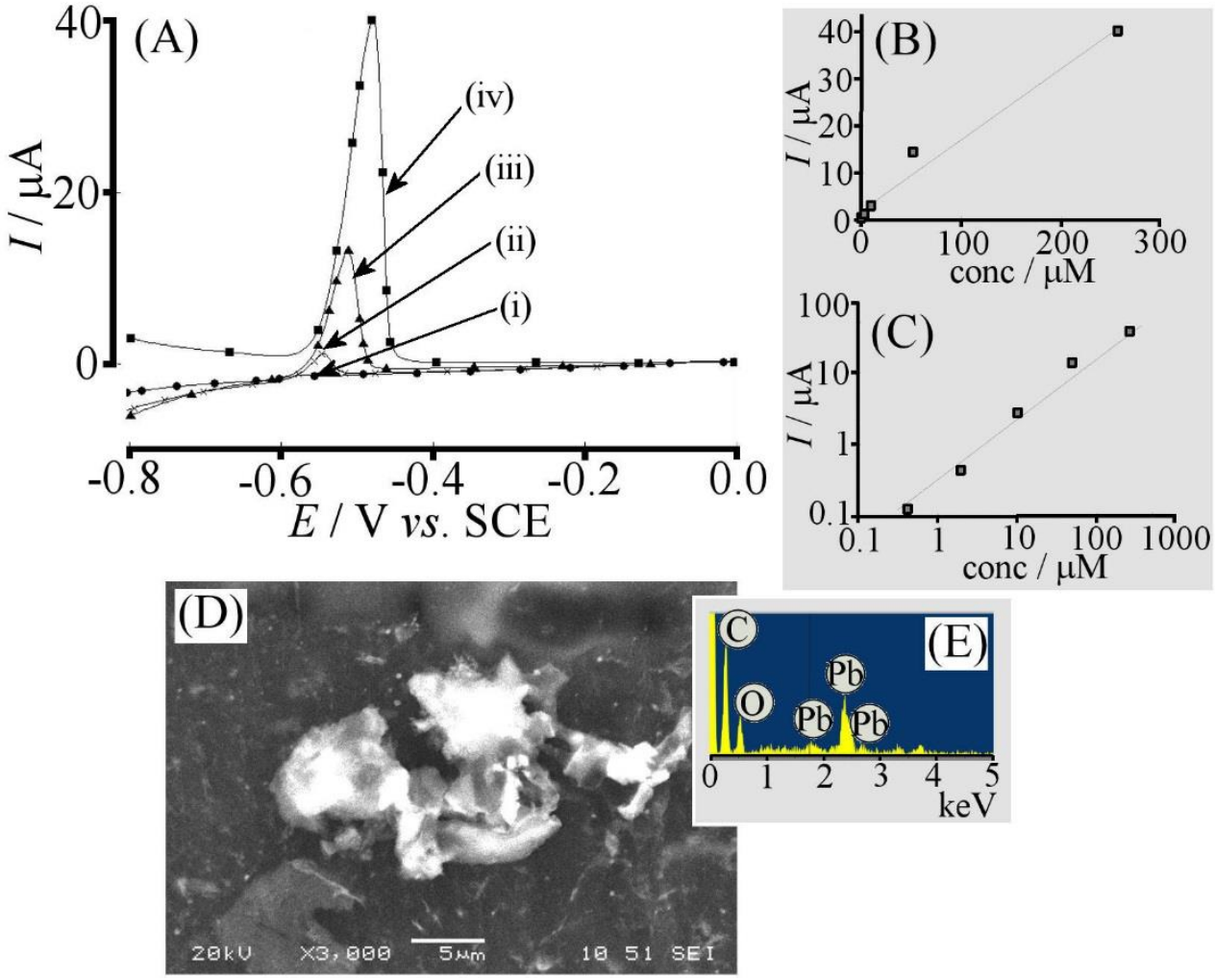

Figure 5. (A) Linear scan differential pulse voltammograms (modulation 50 mV, step potential 5 mV, modulation time 0.1 s, 60 s deposition at -1.0 V vs. SCE) for the anodic stripping detection of (i) 2.1, (ii) 10, (iii) 51, (iv) 258 µM Pb^{2+} in aqueous 0.1 M HNO_3 at a polystyrene/CNF/graphite composite electrode. (B) Plot of the stripping peak current versus concentration and (C) double logarithmic plot. (D) Scanning electron micrograph (SEM) showing a Pb metal deposit on the surface of the composite electrode. (E) EDX data for Pb metal deposit on the composite electrode surface.

Figure 5 shows typical anodic stripping voltammetry data with a characteristic Pb peak at approximately -0.5 V vs. SCE [31]. The peak current can be used as a measure of concentration and a plot of peak current versus concentration appears linear (Figure 5B,C) down to ca. 1 µM Pb^{2+}. Increasing the deposition time can be shown to further enhance the stripping peak response for lower concentrations. Therefore, the performance of the polystyrene/CNF/graphite flake composite electrode is good and comparable to results achieved with other types of carbon materials.

Applications in trace analysis are possible, in particular with further optimisation of the nanocomposite formulation to aid selectivity and pre-accumulation effects [32].

Conclusion

A range of polymers have been tested for application in 3D-printing of electrochemical devices and polystyrene (HIPS) has been identified as the most versatile and best performing matrix material for applications in aqueous media. With 80 wt% polystyrene, 10 wt% carbon nanofibers, 10 wt% graphite flakes a compromise of good electrical conductivity and excellent electrode surface properties with good mechanical and printing characteristics. A combination of pure polystyrene and polystyrene nanocomposite can be employed for complete device prototyping ensuring good interfacing between conductor and shell components. Sufficient dispersion was achieved using solvent blending, and without the use of further additives such as surfactants [33]. Further improvements are possible via more homogenous additive dispersion using mechanical blending methods [34].

The need for new 3D-printing techniques and devices in electrochemistry has been highlighted [6] and the corresponding need for low cost ink formulations extends to smaller print scale (microfluidic devices and chips) and to larger print scale (fuel cells and supercapacitor devices). The polystyrene based filament system developed here is likely to be beneficial in device printing for applications in analytical monitoring of metal pollutants as well as in health-related sensor developments. A major benefit of the composite material is compositional flexibility and the potential for additives to achieve selectivity or to introduce additional functionality.

Acknowledgements

ZR thanks the Engineering and Physical Sciences Council (EPSRC, UK) for funding. PI and RV thank The Royal Society International Exchanges Scheme grant IE141589.

References

[1] B.W. An, K. Kim, H. Lee, S.Y. Kim, Y. Shim, D.Y. Lee, J.Y. Song, J.U. Park, *Adv. Mater.*, **2015**, *27*, 4322-4328.

[2] A. Bellini, S. Güçeri, M. Bertoldi, *ASME. J. Manuf. Sci. Eng.*, **2004**, *126*, 237-246.

[3] G. Scotti, V. Matilainen, P. Kanninen, H. Piili, A. Salminen, T. Kallio, S. Franssila, *J. Power Sources*, **2014**, *272*, 356-361.

[4] S.V. Murphy, A. Atala, *Nature Biotechnol.*, **2014**, 32, 773-785.

[5] S.V. Ley, D.E. Fitzpatrick, R. Ingham, R.M. Myers, *Angew. Chem. Internat. Ed.*, **2015**, *54*, 3449-3464.

[6] M.D. Symes, P.J. Kitson, J. Yan, C.J. Richmond, G.J. Cooper, R.W. Bowman, T. Vilbrandt, L. Cronin, *Nature Chem.*, **2012**, *4*, 349-354.

[7] S. Tsuda, H. Jaffery, D. Doran, M. Hezwani, P.J. Robbins, M. Yoshida, L. Cronin, *PloS ONE*, **2015**, *10*, e0141640.

[8] L. Wang, L. Jing, *Sci. China Technol. Sci.*, **2014**, *57*, 1721-1728.

[9] C. Ladd, J.H. So, J. Muth, M.D. Dickey, *Adv. Mater.*, **2013**, *25*, 5081-5085.

[10] S.J. Leigh, R.J. Bradley, C.P. Purssell, D.R. Billson, D.A. Hutchins, *PLoS ONE*, 2012, *7*, *e49365*.

[11] X. Wang, Q. Guo, X. Cai, S. Zhou, B. Kobe, J. Yang, *ACS Appl. Mater. Interf.*, **2014**, *6*, 2583-2587.

[12] X. Wei, D. Li, W. Jiang, Z. Gu, X. Wang, Z. Zhang, Z. Sun, *Sci. Rep.*, **2015**, *5*, 11181.

[13] C.K. Su, P.J. Peng, Y.C. Sun, *Anal. Chem.*, **2015**, *87*, 6945-6950.

[14] J.L. Erkal, A. Selimovic, B.C. Gross, S.Y. Lockwood, E.L. Walton, S. McNamara, R.S. Martin, D.M. Spence, *Lab on a Chip*, **2014**, *14*, 2023-2032.

[15] G.W. Bishop, J. Satterwhite, S. Bhakta, K. Kadimisetty, K.M. Gillette, E. Chen, J.F. Rusling, *Anal. Chem.*, **2015,** *87*, 5437-5443.

[16] R.L. McCreery, *Chem. Rev*, **2008**, *108*, 2646-2687.

[17] K. Gong, Y. Yan, M. Zhang, L. Su, S. Xiong, L. Mao, *Anal. Sci.*, **2005**, *21*, 1383-1393.

[18] G. Zou, D. Zhang, C. Dong, H. Li, K. Xiong, L. Fei, Y. Qian, *Carbon*, **2006**, *44*, 828-832.

[19] K. Lawrence, C.L. Baker, T.D. James, S.D. Bull, R. Lawrence, J.M. Mitchels, M. Opallo, O.A. Arotiba, K.I. Ozoemena, F. Marken, *Chem. Asian J.*, **2014**, *9*, 1226-1241.

[20] M. Pumera, *Chem. Record*, **2009**, *9*, 211-223.

[21] L. Rassaei, M. Sillanpää, M.J. Bonné, F. Marken, *Electroanalysis*, **2007**, *19*, 1461-1466.

[22] R. Jones, P. Haufe, E. Sells, P. Iravani, V. Olliver, C. Palmer, A. Bowyer, *Robotica*, **2011**, *29*, 177-191.

[23] K. Kalaitzidou, H. Fukushima, L.T. Drzal, *Materials*, **2010**, *3*, 1089-1103.

[24] C.E. Hotchen, I.J. Maybury, G.W. Nelson, J.S. Foord, P. Holdway, F. Marken, *Phys. Chem. Chem. Phys.*, **2015**, *17*, 11260-11268.

[25] A.J. Gross, F. Marken, *Electroanalysis*, **2015**, *27*, 1035-1042.

[26] M. Li, Y.T. Li, D.W. Li, Y.T. Long, *Anal. Chim. Acta*, **2012**, *734*, 31-44.

[27] N.Y. Stozhko, N.A. Malakhova, M.V. Fyodorov, K.Z. Brainina, *J. Solid State Electrochem.*, **2008**, *12*, 1219-1230.

[28] K.C. Honeychurch, J.P. Hart, *TRAC-Trends Anal. Chem.*, **2003**, *22*, 456-469.

[29] D. Omanovic, C. Garnier, K. Gibbon-Walsh, I. Pizeta, *Electrochem. Commun.*, **2015**, *61*, 78-83.

[30] J.H.T. Luong, E. Lam, K.B. Male, *Anal. Methods*, **2014**, *6*, 6157-6169.

[31] F. Marken, M.L. Gerrard, I.M. Mellor, R.J. Mortimer, C.E. Madden, S. Fletcher, K. Holt, J.S. Foord, R.H. Dahm, F. Page, *Electrochem. Commun.*, **2001**, *3*, 177-180.

[32] X.H. Niu, H.L. Zhao, M.B. Lan, *Anal. Sci.*, **2011**, *27*, 1237-1241.

[33] L. Vaisman, H.D. Wagner, G. Marom, *Adv. Colloid Interf. Sci.*, **2006**, *128*, 37-46.

[34] T. Villmow, P. Pötschke, S. Pegel, L. Häussler, B. Kretzschmar, *Polymer*, **2008**, *49*, 3500-3509.